JOURNAL OF GEOPHYSICAL RESEARCH, VOL. 98, NO. C8, PAGES 14,353–14,368, AUGUST 15, 1993

On Mean and Seasonal Currents and Transports at the Western Boundary of the Equatorial Atlantic

FRIEDRICH SCHOTT, JÜRGEN FISCHER, JÖRG REPPIN, AND UWE SEND

Institut für Meereskunde, Universität Kiel, Kiel, Germany

Current measurements from two consecutive yearlong deployments of three moored stations at the western end of the equator in the Atlantic, along 44°W, are used to determine the northwestward flow of warm water in the upper several 100 m and of the southeastward counterflow of North Atlantic Deep Water (NADW). Measurements from three acoustic Doppler current profilers (ADCPs) looking upward from 300 m toward the surface allowed calculation of a time series of upper layer transports over 1 year. Mean transport through the array for the upper 300 m is 23.8 Sv with an annual cycle of only ±3 Sv that has its maximum in June–August and minimum in northern spring. Estimated additional mean northwestward transport in the range 300–600 m is 6.7 Sv, based on moored data and shipboard Pegasus and lowered ADCP profiling. In the depth range 1400–3100 m a current core with maximum annual mean southeastward speed of 30 cm s^{-1} is found along the continental slope that carries an estimated upper NADW transport of 14.2–17.3 Sv, depending on the extrapolation used between the mooring in the core and the continental slope. This transport is higher than off-equatorial estimates and suggests near-equatorial recirculation at the upper NADW level, in agreement with northwestward mean flow found about 140 km offshore. Below 3100 m and above the 1.8°C isotherm, only a small core of lower NADW flow with speeds of 10–15 cm s^{-1} is found over the flat part of the basin near 1.5°N, clearly separated from the continental slope by a zone of near-zero mean speeds. Estimated transport of that small current core is about 4.5 Sv, which is significantly below other estimates of near-equatorial transport of lower NADW and suggests that a major fraction of lower NADW may cross the 44°W meridian north of the Ceara Rise. Intraseasonal variability is large, although smaller than observed at 8°N near the western boundary. It occurs at a period of about 1 month when it is dominant in the near-surface records and corresponds to earlier observations in the equatorial zones of all oceans and at a period of about 2 months when it is dominant at the NADW level and could be imported either from the north along the boundary or from the east along the equator. The existence of an annual cycle in the deep currents of a few centimeters per second amplitude, as suggested by high-resolution numerical model results, could neither be proven nor disproven because of the high amount of shorter-period variability.

1. INTRODUCTION

The thermohaline cell in the North Atlantic is an essential part of the global climate system, but its transports and pathways are still unsatisfactorily determined, especially in the equatorial zone. The magnitude of the meridional overturning transport in the subtropical North Atlantic near 24°N was estimated at 17 Sv [*Roemmich and Wunsch*, 1985], which is approximately required to account for the poleward heat transport of 1.2 PW at that latitude. Nearer to the equator, recent estimates of the transport of the deep western boundary current (DWBC) carrying North Atlantic Deep Water (NADW) southward arrive at even larger numbers: *Speer and McCartney* [1991] obtained 25 Sv from geostrophic calculations based on historical hydrographic data; and *Molinari et al.* [1992], using new hydrographic sections off the north Brazil and Guyana coast in the context of the Subtropical Atlantic Climate Studies program, determined a similarly high mean of 24 Sv from six different sections. The width of the DWBC just north of the equator was determined to about 100 km by recent SOFAR float measurements at the 1800-m-depth level (*Richardson and Schmitz* [1993], hereinafter referred to as RS93), and by combining the horizontal velocity profile at 1800 m with the depth distribution of the DWBC measured by a moored array near 6°N [*Colin et al.*, 1991] they estimated a transport of about 15 Sv for the DWBC above 2600 m. From the offshore float tracks, RS93 concluded that a recirculation out of the DWBC in the western basin north of the equator should exist, leaving only 9 Sv to cross the equator.

There is evidence in transient tracer measurements [*Weiss et al.*, 1991] and reanalyzed salinity and oxygen distributions of the historical hydrographic data set [*Reid*, 1989] that part of the upper NADW arriving at the equator may branch off toward the east along the equator, while the middle and lower NADW appear to continue southward along the western boundary topography. The sparse available data base from the western basin yields conflicting evidence regarding eastward NADW branching along the equator: Pegasus profiles at 35°W show westward flow on the equator in the upper NADW depth range both in October 1990 and June 1991 (M. Rhein et al., manuscript in preparation, 1993); and at 30°W, westward flow was found in June 1991, while *Ponte et al.* [1990] had measured eastward current there in January 1989 [*Böning and Schott*, 1993]. The float measurements of RS93 showed swift eastward currents over several months along the equator which they linked to eastward branching of the DWBC along the equator and westward currents at other times, apparently associated with the DWBC crossing the equator.

The deep flow fields in a seasonally forced high-resolution model show swift seasonally reversing zonal currents at the equator which are absent when the model is forced with constant winds over the equator [*Böning and Schott*, 1993]. Evaluation of the advective and diffusive contributions in

Paper number 93JC01287.
0148-0227/93/93JC-01287$05.00

that model indicated, however, that the maintenance of the tracer wedge along the equator can be accomplished by very small mean eastward currents requiring only a branching off of a very minor fraction of the DWBC.

Although much more is known about the upper layer flow, direct measurements of currents and transports near the equator are rare [*Flagg et al.*, 1986], and a fair amount of uncertainty exists as to the magnitude and pathways of cross-equatorial exchange in the upper 1200 m along the western boundary. It is well established from historical ship drift data [e.g., *Richardson and Walsh*, 1986] that there is a northwestward boundary current along the coast of north Brazil between Cape San Roque and some latitude north of the equator. This boundary current carries the waters across the equator that arrive at the western boundary with the South Equatorial Current (SEC), and it can be connected back both by geostrophic streamlines [*Stramma*, 1991] and by its salinity, oxygen, and nutrient distributions [*Tsuchiya*, 1986; *Reid*, 1989] to the southeastern South Atlantic. The upper layer geostrophic transport arriving off Cape San Roque near 5°S and merging into the northwestern boundary current was found to be of the order of 15 Sv by *Stramma* [1991]. More westward flow joins between 5°S and the equator from the SEC.

Near the equator and to the north of it the North Brazil Current (NBC) feeds three zonal current systems [e.g., *Cochrane et al.*, 1979]: the Equatorial Undercurrent (EUC), the North Equatorial Undercurrent (NEUC) in the latitude range 3°–5°N, and the North Equatorial Countercurrent (NECC) at 5°–8°N. How much NBC flow continues northward along the boundary is presently unclear. In late summer to fall, the NBC retroflects near 5°–8°N (*Richardson and Walsh* [1986] and *Johns et al.* [1990], hereinafter referred to as J90, with most of its cross-equatorial transport apparently merging into the eastward flowing NECC. In late winter to spring, the NECC weakens, and surface currents are disorganized and even reversed in the western tropical Atlantic north of the equator [*Richardson and Reverdin*, 1987]. The consequence was thought to be a maximum of northwestward flow along the coast toward the Caribbean in late winter [*Richardson and Philander*, 1987], but evidence for this circulation scheme could not be found in the altimetry signal along the South American coast [*Didden and Schott*, 1992]. Overall, currents toward the Caribbean north of the retroflection zone appear to be small in both seasons. Yet waters of clearly South Atlantic origin are getting into the Caribbean and toward the Florida Current [*Schmitz and Richardson*, 1991]. There are two other possible routes for the mean water mass transfer from the South Atlantic to the Caribbean besides mean flow along the boundary. First, the NBC/NECC pathway: this is also in agreement with the tropical Atlantic Sverdrup circulation which has approximately 10–20 Sv (depending on the wind stress climatology used) turning offshore north of the equator and returning via the North Equatorial Current (NEC) toward the Caribbean [e.g., *Böning et al.*, 1991]. Second the NBC/NECC retroflection zone is known to shed eddies which can be traced propagating northwestward along the Guyana coast [*Didden and Schott*, 1993; J90] and could contribute significantly to the interhemispheric water mass transfer. The picture could be complicated further by the presence of a southward coastal undercurrent that was first found in the circulation pattern of the high-resolution WOCE model [*Schott and Böning*, 1991] where it carried high-salinity water from near the eastern Caribbean toward the equator in the depth range 100–300 m. Subsequent evidence from climatological data analysis of this feature was found by E. Johns and R. L. Molinari (personal communication, 1992).

To measure the boundary currents and transports at the equator, a program with moored stations along the continental slope at the intersection of the 44°W meridian and the equator (Figure 1) was carried out from October 1989 to September 1991 with a deployment of three moorings each year, where the shallowest mooring, at 545 m depth at position A, was a repeat deployment of an upward looking 150-kHz acoustic Doppler current profiler (ADCP) at 250 m depth. The second-year array also carried upward looking ADCPs at 250 m depth at positions B and D. The three ADCPs from the second deployment allow determination of a yearlong cross-equatorial transport time series for the near-surface flow.

The resolution of the array at the NADW levels, both meridionally and vertically, is still too coarse to present reliable means or transport time series but will allow estimates of upper NADW transport within some bounds. An interesting aspect, also addressed in this paper, is the penetration of the seasonally forced signal. It was found to dominate the deep flow in the WOCE-CME model, but it can only be detected with confidence in the upper layer here. The currrent records contain energetic fluctuations in the period range of several weeks with rms amplitudes of about 40 cm s^{-1} near the surface and 20 cm s^{-1} in the DWBC. These, however, will be considered noise in the context of this paper, and their kinematics and possible sources will be addressed elsewhere.

2. OBSERVATIONS

The first array, moorings K327–K329 on positions A, C, and E (Figure 1), was deployed September 4–6, 1989, with NOAA's vessel *Malcolm Baldrige* and retrieved October 8–10, 1990, on *Meteor* cruise M14 (Table 1). This array carried one ADCP at position A that yielded good data and one on K329 that failed after 36 hours because of a recorder problem (when restarted after retrieval, it worked fine). Moorings on positions C and E carried a total of 14 Aanderaa current meters (ACMs), but as a result of excessive power consumption of new and refurbished instruments, substantial data losses were experienced in that deployment.

The second array, moorings K339–K341 on positions A, B, and D, was deployed on cruise M14/2 during October 12–13, 1990. The three upward looking ADCPs at 300-m depth yielded good data, and useful records were obtained from 12 ACMs. Recording time interval was 2 hours on the ACMs and 1 hour on the ADCPs. The ADCPs had a vertical bin length of 8.7 m and an ensemble consisted of 200–400 pings, differing among the ADCPs, which were transmitted at 1-s time interval. The corresponding standard deviation of each ensemble due to acoustic noise for the horizontal velocity was 1.4–1.0 cm s^{-1} [*RD Instruments*, 1989]. The depth of the ADCP was determined for each ensemble from the distance off the surface measured by the surface backscatter, and time series were reassembled for constant depth levels by rearranging bin data to actual depths. In comparing ADCP currents with ACM currents in the following, this means that the former are from fixed depths and the latter are from varying depths, sometimes with excursions exceeding 100 m.

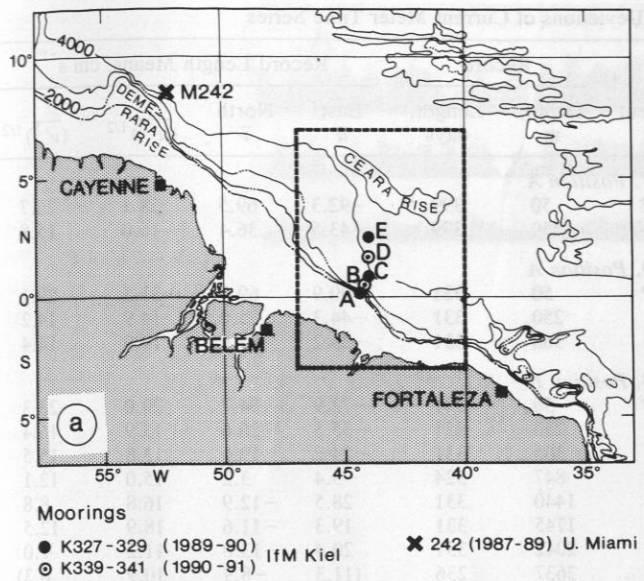

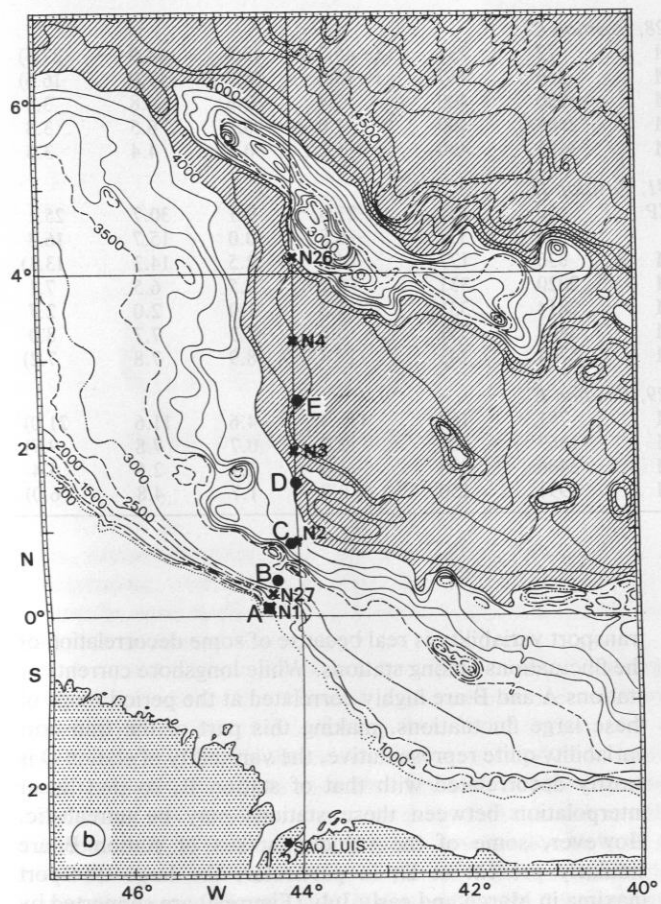

Fig. 1 (*a*). Topography of western equatorial Atlantic and location of IfM Kiel moorings K327–K329 (positions A, C, and E), K339–341 (positions A, B, and D), and mooring 242 of *Johns et al.* [1990]. Inset is location of Figure 1*b*. (*b*) Detailed topography around array including Ceara Rise including moored stations A to E and positions (N.. etc.) of Pegasus profiling.

Since we will focus in the following on the mean and seasonal signal with some statistical information also on the variability at the time scale of weeks to months, the short-period fluctuations including the tidal signal have been filtered out by applying a Lanczos filter with a 40-hour cutoff period to all time series. These are shown in Figure 2 except for station E, for which three of the four records obtained were only about 5 months long (Table 1). Vector means are shown in Figure 3, and the section distribution of the current component parallel to the topography is shown in Figure 4. The mean near-surface current decreases from more than 1 m s^{-1} at the shelf edge station to about 20 cm s^{-1} at the offshore station D, indicating that the ADCP array covered most of the near-surface transport. An interesting result is that the current vector time series for the combined record at position A over the 2-year deployment period (Figure 2*a*) shows only indications of a seasonal variation very near to the surface with apparent maxima in late summer and minima in spring to early summer. This seasonal signal disappears below about 100 m, and the currents are dominated by the shorter-period fluctuations.

The measurements near 800 m, i.e., in the Antarctic Intermediate Water (AIW) range, show weak northwestward flow near the boundary (Table 1), not recognizable as a boundary current on the background of the fluctuations of 15 cm s^{-1} rms amplitude (Figure 2*b*). Below, at depths between 1400 m and 2700 m along the continental slope (station B, Figure 2*b*) the current is steady southeastward with rare occasions of reversal. Maximum mean speed parallel to the topography at the upper NADW core depth is 30 cm s^{-1} (Figures 3*a* and 4 and Table 1). At station D at 1°33′N, the current at 2020 m is northwestward almost throughout the entire year with only a few weak reversals (Figure 2*d*), suggesting steady recirculation at the offshore side of the upper DWBC.

An identifiable lower NADW core is not observed along the continental slope, but away from the continental rise, at the deepest two instruments of station D, southeastward flow, with almost no reversals during the year (Figure 2*d*) and a mean of 15 cm s^{-1} 300 m above the bottom, is observed. In contrast, at station C further toward the topography, currents are fluctuative (Figure 2*c*) with near-zero mean (Figure 4).

During *Meteor* cruises M14/2 and M16/3, hydrographic sections including Freon (F11) sampling [*Rhein*, 1993] and velocity profiling were carried out along the 44°W section (Figure 1*b*). Besides shipboard ADCP, velocity profiles on station were obtained by Pegasus and by self-contained ADCP attached to the conductivity/temperature/depth sonde (CTD). While Pegasus yields absolute currents, the profiles from the lowered ADCP are constructed by strapping the shears piecewise together to obtain a total shear profile that is then referenced by the Global Positioning System. This latter method and its accuracy are discussed elsewhere [*Fischer and Visbeck*, 1993]. It compared well with Pegasus profiles, at least in the upper 1000 m. We will use profiling data from both methods for comparison with the moored measurements and interpretation of the spatial scales of the currents around the array.

3. Transport Estimates

3.1. *Near-Surface Layer*

From the profiles of the moored ADCPs at stations A, B, and D, transport time series for the upper 300 m were calculated. As stated earlier, the ADCP profiles were reas-

TABLE 1. Overall Means and Standard Deviations of Current Meter Time Series

Position	Water Depth, m	Deployment Period	Instrument Sequence	Instrument Type	Record Depth, m	Record Length, days	Record Length Means, cm s^{-1} East $\bar{u}$	North $\bar{v}$	$(\overline{u'^2})^{1/2}$	$(\overline{v'^2})^{1/2}$
				Mooring K327, Position A						
0°5.2′N, 44°23.2′W	545	Sept. 6, 1989–Oct. 10, 1990	32701	ADCP	50	399	−92.3	69.5	28.1	26.7
					250	399	−43.5	36.4	16.0	15.8
				Mooring K339, Position A						
0°5.2′N, 44°23.2′W	545	Oct. 12, 1990–Sept. 8, 1991	33901	ADCP	50	331	−90.9	69.0	31.5	29.1
					250	331	−44.3	35.0	14.9	14.2
			33902	ACM	368	331	−23.2	22.6	14.9	14.4
				Mooring K340, Position B						
0°25.2′N, 44°15.0′W	3340	Oct. 12, 1990–Sept. 8, 1991	34001	ADCP	50	331	−72.9	54.7	20.0	23.3
					250	331	−35.5	26.6	13.9	16.4
			34002	ACM	305	331	−24.2	19.0	13.8	15.5
			34003	ACM	847	324	−3.4	3.2	15.0	12.1
			34004	ACM	1440	331	28.5	−12.9	16.8	8.8
			34005	ACM	1745	331	19.3	−11.6	18.9	12.5
			34006	ACM	2042	331	20.4	−13.0	11.2	7.0
			34007	ACM	2637	236	(11.3	−8.9	10.9	6.3)
			34008	ACM	3235	331	3.5	−1.7	3.3	2.4
				Mooring K328, Position C						
0°50′N, 44°04.3′W	3989	Sept. 5, 1989–Oct. 11, 1990	32801	ACM	72	231	(−45.3	43.8	14.9	27.5)
			32802	ACM	246	167	(−15.8	8.7	17.9	16.6)
			32805	ACM	1990	400	3.4	−2.6	6.8	3.8
			32806	ACM	2588	400	1.6	−0.3	6.5	3.8
			32808	ACM	3695	400	−1.2	−0.1	4.4	3.3
				Mooring K341, Position D						
1°33′N, 44°0.7′W	4108	Oct. 13, 1990–Sept. 9, 1991	34101	ADCP	50	331	−21.5	9.1	30.7	25.1
					250	331	−6.8	0.0	15.7	16.3
			34102	ACM	830	177	(4.6	−2.5	14.3	13.1)
			34104	ACM	2020	331	−6.2	4.5	6.5	7.1
			34105	ACM	2814	331	−1.3	1.0	2.0	2.7
			34106	ACM	3409	331	8.6	−7.3	7.7	8.0
			34107	ACM	3704	245	(13.4	−8.9	7.8	7.2)
				Mooring K329, Position E						
2°29′N, 43°58′W	4191	Sept. 4, 1989–Oct. 8, 1990	32902	ACM	781	150	(11.4	−4.6	11.6	21.0)
			32903	ACM	1369	162	(2.5	0.7	7.8	9.9)
			32905	ACM	3486	398	−1.0	2.9	2.5	6.4
			32906	ACM	3991	150	(−0.7	1.7	4.8	6.0)

Parentheses indicate reduced record length.

sembled for constant depth. For calculating the transports across the line of moorings, the currents were rotated onto the direction normal to the mooring line segments A/B (distance 41 km) and B/D (distance 129 km), respectively. For the upper 50 m, where ADCP data are affected by surface bias backscatter, two extrapolations were used. First, the top values from 50 m were applied for this layer representing slab motion of the top layer. Second, the instantaneous profiles between 150 m and 50 m were used for a line fit which was then extrapolated to the surface. Mean section transport for the upper 300 m from the 500-m-depth contour (station A) out to 170 km (station D) is 23.8 ± 4.6 Sv for the line fit extrapolation case and only slightly lower (23.5 Sv) for the constant extrapolation case. The inner pair of moorings (out to 41 km) contributes about one third, 8.3 Sv, to the mean transport (Table 2). About half of the transport in the ADCP range is carried in the upper 100 m and only 21% in the 200- to 300-m range.

Fluctuations of the transport time series on the time scale of several weeks are large, with total transport ranging from 14 Sv to 38 Sv (Figure 5). Not all of this short-period transport variability is real because of some decorrelation of the fluctuations among stations. While longshore currents of stations A and B are highly correlated at the period range of these large fluctuations, making this part of the transport variability quite representative, the variability of station D is mostly decorrelated with that of station B, so that linear interpolation between these stations may be unrealistic. However, some of the velocity spikes of station B are similarly present at D; in particular, the large transport maxima in March and early July (Figure 5) are supported by all three stations.

It is difficult to judge how much mean warm water transport escapes on both sides of the array and below 300 m. Shipboard ADCP sections across the shelf were carried out with R/V *Meteor* both in October 1992 and in June 1991. Currents ranged from 25 to 50 cm s^{-1}, and total transport across that shelf section toward the NW was only about 0.5 Sv in both cases. This low value is in contrast to the 2.3 and 3.0 Sv obtained by *Candela et al.* [1992] from two ADCP shelf surveys farther northwest at 48°–52°W (May and March, respectively). In the southeast of their survey area,

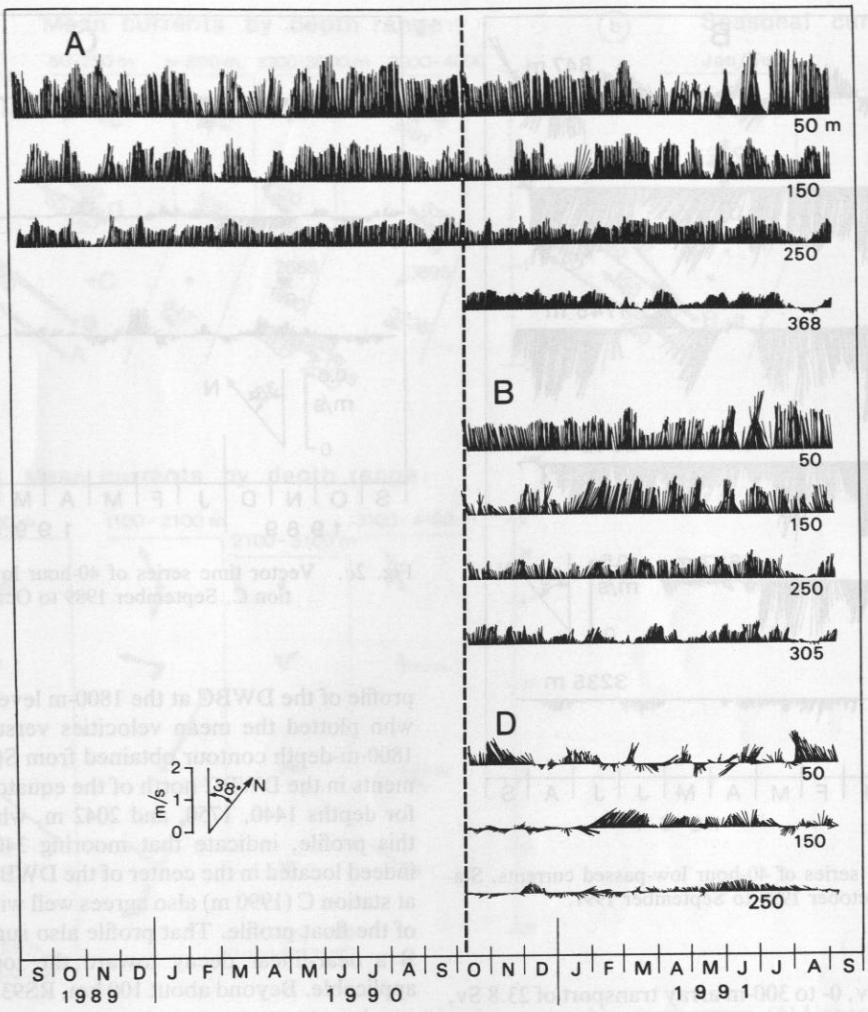

Fig. 2*a*. Vector time series of 40-hour low-passed currents. September 1989 to September 1991 in upper layer; records from upper 250 m are by ADCPs.

i.e., toward our site, their ship transports were drastically decreasing, which suggests that the NBC flow penetrates onto the shelf north of the Amazon exit where the coastline curves northward (Figure 1*a*).

A current section, measured with lowered ADCP during May 23–25, 1991, from the shelf edge to about 5°N is shown in Figure 6. The NBC during this 2-day period has a subsurface westward maximum located at 250–300 m depth and an eastward current core above it, separating it from the westward surface flow. The current structure is also apparent from Figure 2*a* for these days (except for lack of a complete reversal to eastward at the 100–150 m level that is smoothed out in Figure 2*a* by low-pass filtering but apparent in the unfiltered data), but it is not representative of mean spring conditions. The NBC decays to 500 m in the vertical and in the horizontal to 2°N at the offshore side in that ship section.

The ship section transport above 300 m and to 2°N from the M16 cruise is marked in Figure 5 for comparison, determined by both Pegasus (18.7 Sv) and lowered ADCP (16.9 Sv, where shear extrapolation from 34 m depth to the surface is applied), resulting in good agreement with the transport minimum obtained from the moorings at that time. The additional westward transport from Pegasus (ADCP) in the 300–600 m depth range is 6.2 Sv (3.7 Sv). The differences between Pegasus and ADCP reflect partially measurement errors and partially aliasing by higher frequency motions (internal waves) that resulted sometimes in significant differences between upcast and downcast profiles.

During deployment of the array in October 1990 a Pegasus section was also carried out, resulting in a transport of 34.1 Sv south of 2°N (Figure 5) which is higher than the transport maximum determined from the initial data of the mooring time series. This time, though, Pegasus showed much deeper-reaching currents than in Figure 6, which would add an increment of 11.0 Sv in the 300- to 600-m layer. The two ship sections were taken at approximate times of maxima and minima of the 0–300 m transport time series (Figure 5). Averaging the transports of these two extremes plus that of a third *Meteor* cruise, M22/3 of October 1992, yields a transport value for the 300- to 600-m layer of 6.7 Sv, which we will take as an estimate of the mean for this layer. An additional small increment to the moored transports in the 0- to 300-m layer is due to the currents north of station D (1°33′N). Applying a linear offshore decrease from the profile at D (Figure 4) to zero at 2°N would add only 0.9 Sv to the mean transport. Hence estimated total mean transport of warm water above 600 m is 31.9 Sv, made up by the shelf

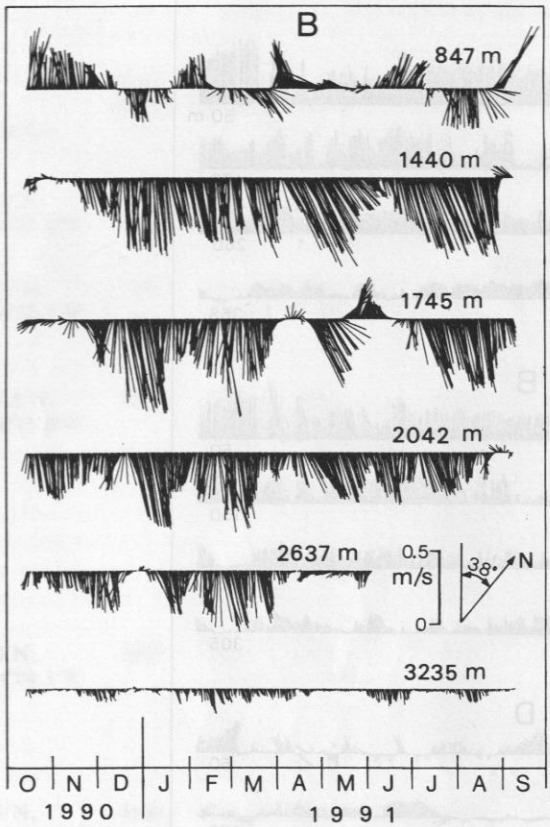

Fig. 2*b*. Vector time series of 40-hour low-passed currents. Station B, October 1990 to September 1991.

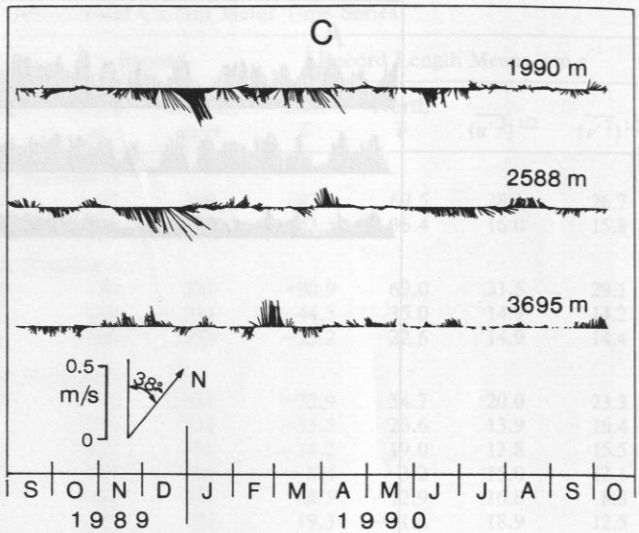

Fig. 2*c*. Vector time series of 40-hour low-passed currents. Station C, September 1989 to October 1990.

contribution of 0.5 Sv, 0- to 300-m array transport of 23.8 Sv, estimated 300- to 600-m extension of 6.7 Sv, and 0- to 300-m offshore fraction of 0.9 Sv.

There must also be flow into the northern hemisphere at the AIW level, where the mean current measured below the salinity minimum, which is located near the array at about 700 m depth, is 5 cm s^{-1} northwestward at station B (Figures 3*a* and 4). At stations D and E the flow is into the opposite direction, but both records are short, 5 and 6 months, respectively. The profiling section of May 1991 (Figure 6) actually showed southeasterly flow near the boundary in the depth range 600–800 m, while in October 1990 the flow next to the boundary was westward but in a much larger depth range than just the AIW level and suggestive of anticyclonic circulation (Figure 3*c*). With no spatial resolution available in the array along the boundary around the AIW layer and conflicting results from the ship sections, transport determination is not possible for that layer.

3.2. *NADW Layer*

In the upper NADW layer, between 1400 and 2100 m, records from station B show a maximum mean speed of about 30 cm s^{-1}, indicating that this mooring must have been located near the core of the current (Figures 3*a* and 4). The current decayed the next 46 km out to station C to just a few centimeters per second, while at station D, 128 km from B, a fairly persistent counterflow of 8 cm s^{-1} mean speed was measured at 2020 m.

For comparison, a measure of the mean cross-stream profile of the DWBC at the 1800-m level was given by RS93, who plotted the mean velocities versus distance from the 1800-m-depth contour obtained from SOFAR float displacements in the DWBC north of the equator. Our annual means for depths 1440, 1750, and 2042 m, when superimposed on this profile, indicate that mooring 340 at position B was indeed located in the center of the DWBC. The measurement at station C (1990 m) also agrees well with the offshore decay of the float profile. That profile also suggests that from stat. B a near-linear decay toward the topography should be applicable. Beyond about 100 km, RS93 obtain a counterflow

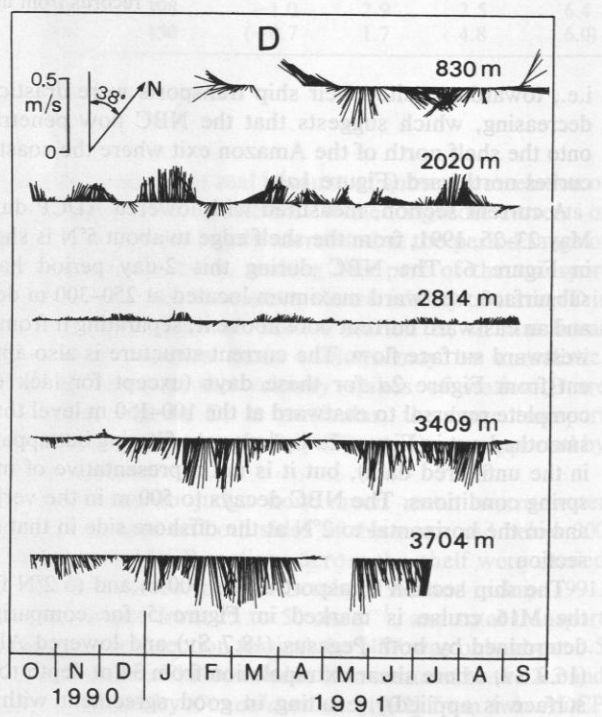

Fig. 2*d*. Vector time series of 40-hour low-passed currents. Station D, October 1990 to September 1991.

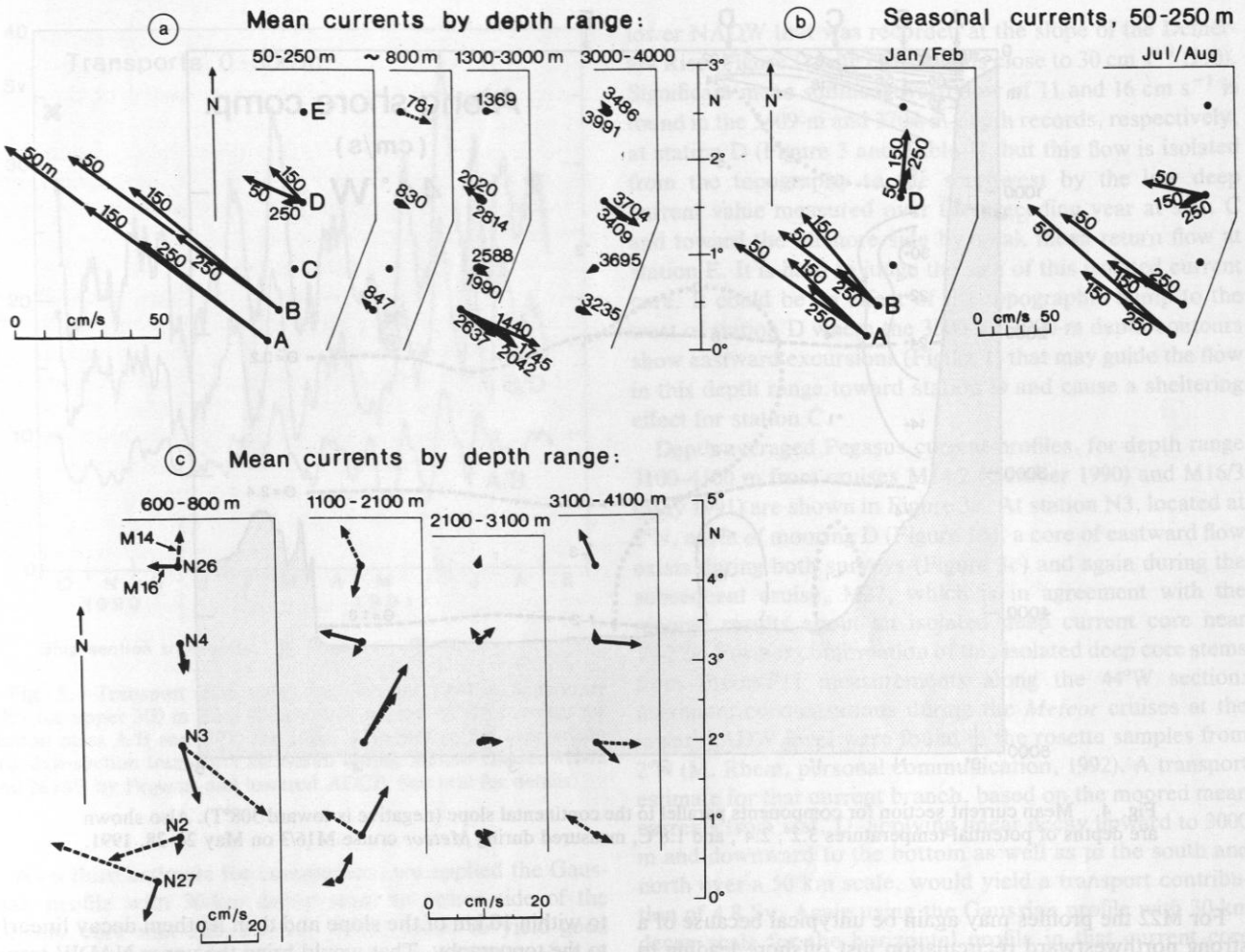

Fig. 3. (*a*) Record length vector means along the mooring line, grouped by depth ranges. (*b*) Upper layer current means from moored ADCP measurements in January/February and July/August 1991. (*c*) Vertically averaged currents by depth ranges measured by Pegasus during *Meteor* cruises M14 (October 10–12, 1990; dashed vectors) and M16 (May 23–25, 1991; solid vectors).

in qualitative agreement with our -8 cm s^{-1} mean at station D (Figures 2*d* and 7).

Our own shipboard current-profiling sections yield somewhat untypical data for determining the width of the upper DWBC. Cruises M14/2 in October 1990 and M16/3 during May 23–25, 1991, both fell into anomalous periods of upper NADW flow. During M14/2, at the beginning of station B records, the currents at station B were particularly weak at 1440- and 1745-m depth (Figure 2*b*), and at the time of cruise M16/3, moored currents at station B were strongly decreasing and even reversing to northward at 1745 m depth (Figure 2*b*). Pegasus layer means for 1100–2100 m from M16/3 show a dominant northward component with a maximum at 2°N, turning to westward at 3°15′N; and for cruise M14/2, vector means over 1100–2100 m near the boundary were northward and also offshore at 2°N (Figure 3*c*). The 2100- to 3100-m means were very small for both cruises near the boundary (Figure 3*c*). In general, the DWBC structure near the boundary at 44°W in Pegasus and lowered ADCP profiles is much more complex than farther north off Guyana, where a large vertical scale of the currents is observed in individual profiles [*Colin et al.*, 1992; *Johns et al.*, 1993]. Ship sections showed multiple cores between 1000 and 3000 m: during M14, eastward cores near the boundary were located at 1400–1600 m and 2000–2400 m; during M16, eastward boundary flow occurred at depths of 1000–1500 m and 2000–2600 m; and during M22, eastward flow was observed at 1600–2700 m. This higher vertical-wavenumber variability may be related to the "stacked jets" that were also observed in the tropical Atlantic at 30°W [*Ponte et al.*, 1990].

For comparison with the float-derived mean profile across the DWBC close to the boundary the alongshore velocities across the eastward current cores near the boundary from cruises M16 and M22 are inserted into Figure 7*a*; M14 is not used because of sparse station coverage along 44°W. Currents from Pegasus and lowered ADCP are vertically averaged over 100-m intervals out of the eastward cores, and the alongshore current values are plotted against the distance of the measurement in that particular depth range from the continental slope. For the M16 data the about linear offshore decay off the float profile from the DWBC core out to about 90 km from the slope is reproduced, although with lower amplitudes due to the generally weaker flow of that period. What is noteworthy is that the highest values are obtained closer to the boundary than in the float profile, i.e., at only 10–15 km distance.

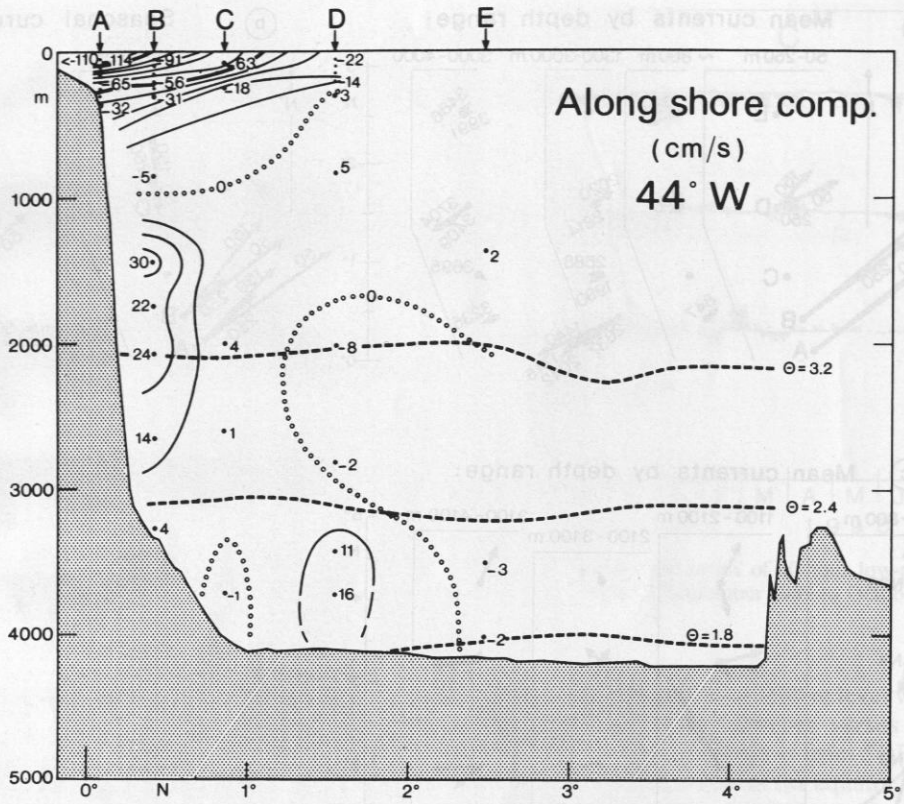

Fig. 4. Mean current section for components parallel to the continental slope (negative is toward 308°T). Also shown are depths of potential temperatures 3.2°, 2.4°, and 1.8°C, measured during *Meteor* cruise M16/3 on May 24–28, 1991.

For M22 the profiles may again be untypical because of a strong northwestward recirculation just offshore leading to negative values already at 50 km offshore. These data therefore are not representative of the offshore decay, but they are shown as a confirmation for the location of the DWBC current core closer to the topography than indicated by the float profile.

On the basis of the above profile discussion we will estimate the transport with three different offshore profiles. First, we use the mean longshore currents from station B (Figure 4), with linear decay toward the topography at each level as suggested by the float profile. Setting for the integration the upper limit of the DWBC at 1000 m yields a total transport in the depth range 1000–3250 m from the continental slope out to station B of 4.7 Sv taken over the eastward current cores near the boundary. A second alternative for extrapolating from station B toward the topography is to take the moored mean currents at constant values to within 10 km of the slope and then let them decay linearly to the topography. That would bring the upper NADW transport between mooring B and the topography up to 7.5 Sv.

At the offshore side (station C) the velocity is 4 cm s^{-1} at 1900-m depth and near-zero at 2588 and 3695 m. For the integration we assume now that the profile above 1990 m is roughly proportional to station 340; that is, the velocities are 4 cm s^{-1} at 1750 m and 5 cm s^{-1} at 1440 and then drop off to zero at 1200 m. The total transport for the 46-km segment between stations B and C thus obtained in the depth range 1000–3250 m is 9.5 Sv. There may be a bit of southeastward NADW transport still north of station C, but the drifter velocity profile (Figure 7*a*) suggests that this should be small. Hence the total NADW transport obtained between the coast and 0°50′N, i.e., about 70 km out from the 1800 m depth contour, lies between 14.2 Sv and 17.0 Sv depending on how the extrapolation from station B toward the topography is carried out.

TABLE 2. Upper Layer Transport Estimates

Upper Layer*	0–41 km	41–170 km	Total		
			Mean	Dec.–Feb.	June–Aug.
0–100	3.8	7.1	10.9	10.2	13.9
100–200	2.7	5.1	7.8	7.6	8.4
200–300	1.8	3.3	5.1	4.2	5.5
0–300	8.3	15.5	23.8 ± 4.6	22.0 ± 3.2	27.8 ± 4.4

Estimates in sverdrups (1 sverdrup = 10^6 m^3 s^{-1}).
*From 500-m-depth contour to 170 km out, linear fit case.

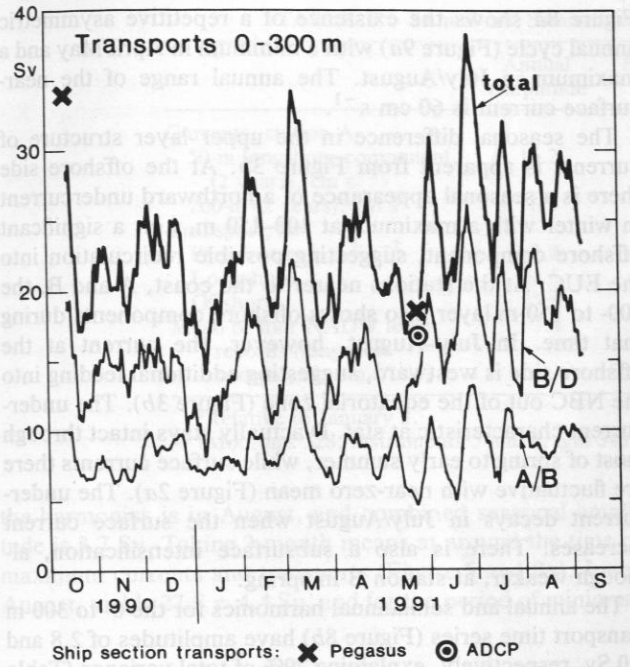

Fig. 5. Transport time series for October 1990 to September 1991 for upper 300 m from 40-hour low-passed ADCP currents for station pairs A/B and B/D, and total. Also plotted for comparison are ship section transports measured during *Meteor* cruises M14/2 and M16/3 by Pegasus and lowered ADCP. See text for details.

As a third estimate for comparison, we applied the Gaussian profile with 30-km decay scale to either side of the current core that *Johns et al.* [1993] found to yield good agreement with the geostrophic transports of *Molinari et al.* [1992] when applied to the mean currents of their station 242 (Figure 1*a*) below 2500 m. It also fits the mixture of shipboard and moored observations well in our case. The transport for this case, when integrating out to the 2 cm s^{-1} contour in the north and to the continental slope in the south, yielded 7.7 Sv shoreward of station B and a total of 17.6 Sv, in close agreement with the higher one of our two linear extrapolation methods.

Still farther out, at station D, the mean is northwestward at 2020 m, suggesting possible recirculation. Recirculation on the offshore side is also suggested by the Pegasus profiles in the upper DWBC ranges (Figure 3*c* and 7*a*) and by water mass distributions, where the Freon/F11 maximum along 44°W extends northward to beyond 3°N.

The NADW transport estimate still does not include the lower NADW that was recorded at the slope of the Demerara Rise (Figure 1) with core speeds close to 30 cm s^{-1} (J90). Significant mean southeastward flow of 11 and 16 cm s^{-1} is found in the 3409-m and 3704-m-depth records, respectively, at station D (Figure 3 and Table 1), but this flow is isolated from the topography to the southwest by the low deep current value measured over the preceding year at stat. C and toward the offshore side by weak mean return flow at station E. It is hard to judge the size of this isolated current core. It could be an effect of the topographic bump to the west of station D where the 3500- to 3900-m depth contours show eastward excursions (Figure 1) that may guide the flow in this depth range toward station D and cause a sheltering effect for station C.

Depth-averaged Pegasus current profiles, for depth range 3100–4100 m from cruises M14/2 (October 1990) and M16/3 (May 1991) are shown in Figure 3*c*. At station N3, located at 2°N, north of mooring D (Figure 1*b*), a core of eastward flow exists during both surveys (Figure 3*c*) and again during the subsequent cruise, M22, which is in agreement with the moored results about an isolated deep current core near 1°–2°N. Further confirmation of this isolated deep core stems from Freon/F11 measurements along the 44°W section: maximum concentrations during the *Meteor* cruises at the lower NADW level were found in the rosette samples from 2°N (M. Rhein, personal communication, 1992). A transport estimate for that current branch, based on the moored mean currents from stat. D, applying linear decay upward to 3000 m and downward to the bottom as well as to the south and north over a 50 km scale, would yield a transport contribution of 4.8 Sv. Again using the Gaussian profile with 30-km decay scale for the horizontal profile in that current core results in the quite similar value of 4.3 Sv.

This is, of course, not all of the lower NADW transport. Since the sill depth between the Ceara Rise and the western continental slope lies between 4000 and 4100 m (Figure 1*b*), part of the lower NADW transport will pass to the north of Ceara. Station resolution on M14 and M16 was too coarse to resolve the deep boundary current along the northern slope of Ceara, but a rough estimate during M22 for the lower NADW transport was about 7 Sv. There may also be further eastward flow south of the Ceara Rise: a current core was found in the profiles of M16 at 3°15′N (Figure 3*c*) and again during M22 while at the southern slope of the Ceara rise; at profiling station N26 (Figure 1) the flow was westward during M16 (Figure 3*c*) and M22, but this eastward core requires further confirmation.

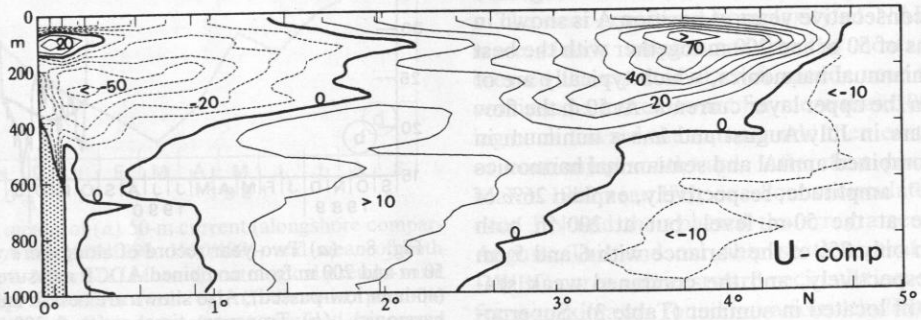

Fig. 6. Section of zonal velocity component for depth range 0–1000 m, May 23–25, 1991, measured by lowered ADCP.

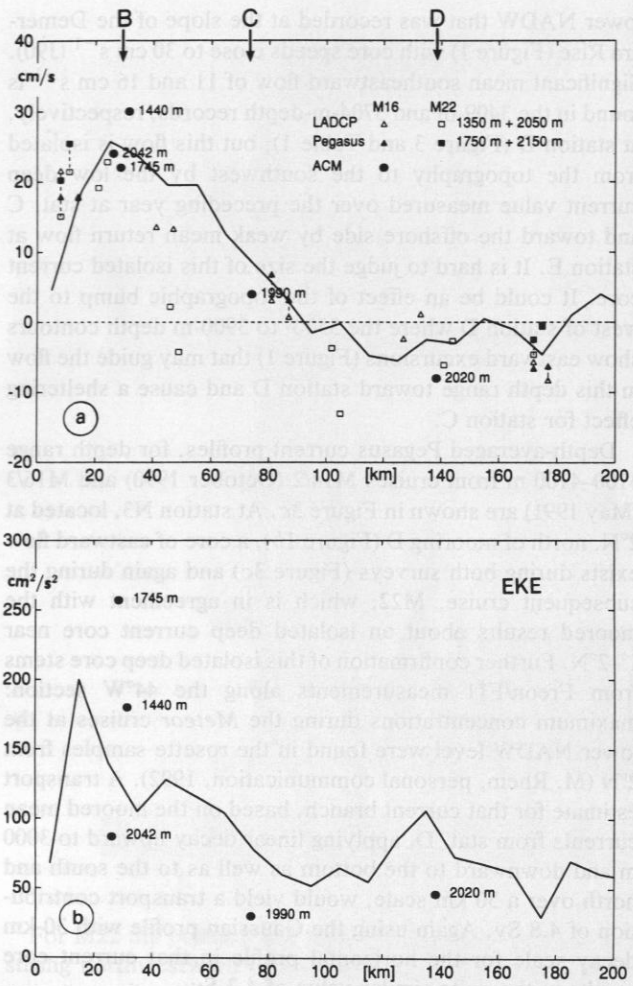

Fig. 7. (*a*) Alongshore mean velocity of the DWBC at 1800 m, determined from SOFAR floats (solid curve, taken from *Richardson and Schmitz* [1993, Figure 6a]) and annual mean currents at upper NADW depths of stations B, C, and D versus distance from respective depth contour. Also shown are currents from eastward current cores, averaged over 100-m layers for center depths as indicated; measured during M16 and M22 with Pegasus and lowered ADCP. Dashed vertical lines connect simultaneous Pegasus and lowered ADCP measurements from same depth layer. (*b*) Same as Figure 7*a* but for eddy kinetic energy (EKE); only current meter EKEs are shown with float EKE line.

4. SEASONALITY AND SHORTER-PERIOD VARIABILITY

4.1. *Near-Surface Layer*

The energetic fluctuations in the period range of several weeks make the identification of an annual cycle in the records and of its depth penetration difficult. The alongshore velocity for both consecutive years at position A is shown in Figure 8 for depths of 50 m and 200 m together with the best fit annual and semiannual harmonics, which typically are of equal magnitude in the upper layer currents. At 50 m the flow is higher both years in July/August and has a minimum in April/May. The combined annual and semiannual harmonics of 16 and 19 cm s^{-1} amplitude, respectively, explain 26% of the total variance at the 50-m level, but at 200 m both harmonics explain only 7% of the variance with 6 and 5 cm s^{-1} amplitude, respectively, and the combined weak seasonal maximum still located in summer (Table 3). Superposition of the monthly means for the 50 m depth currents from Figure 8*a* shows the existence of a repetitive asymmetric annual cycle (Figure 9*a*) with a minimum in April/May and a maximum in July/August. The annual range of the near-surface current is 60 cm s^{-1}.

The seasonal difference in the upper layer structure of currents is apparent from Figure 3*b*. At the offshore side there is a seasonal appearance of a northward undercurrent in winter with a maximum at 100–150 m, i.e., a significant offshore component, suggesting possible recirculation into the EUC. At the stations nearer to the coast, A and B, the 100- to 150-m layer also shows offshore components during that time. In July–August, however, the current at the offshore side is westward, suggesting additional feeding into the NBC out of the equatorial zone (Figure 3*b*). The undercurrent characteristic at stat. D actually stays intact through most of spring to early summer, while surface currents there are fluctuative with near-zero mean (Figure 2*a*). The undercurrent decays in July/August when the surface current increases. There is also a subsurface intensification, although weaker, at station B in spring.

The annual and semiannual harmonics for the 0- to 300-m transport time series (Figure 8*b*) have amplitudes of 2.8 and 2.0 Sv, respectively, explaining 29% of total variance (Table 3), where one has to be reminded that there may be a fraction of noise in the 1- to 2-month period band due to insufficient horizontal resolution. The combined seasonal maximum of

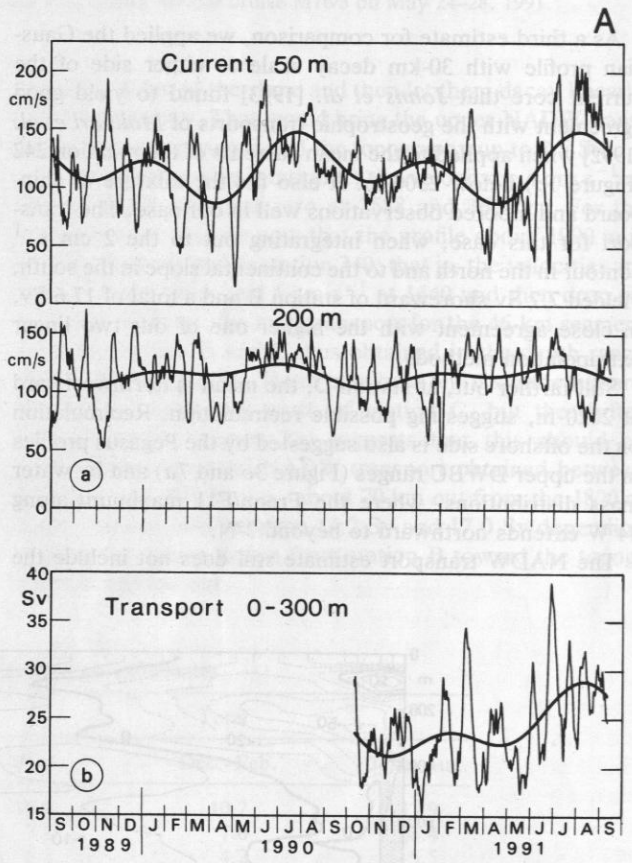

Fig. 8. (*a*) Two-year record of alongshore velocity at depths of 50 m and 200 m from combined ADCP measurements at position A (40-hour low-passed). Also shown are best fit annual and semiannual harmonics. (*b*) Transport time series 0–300 m with annual and semiannual harmonics.

TABLE 3. Annual and Semiannual Harmonics of Currents and Transports

	Annual Amplitude	Phase,* deg	Semiannual Amplitude	Phase,* deg	Total Variance Explained, %
Currents, station A					
50-m longshore component (2 years), cm s^{-1}	16.2	235	19.3	34	26
200-m (2 years), cm s^{-1}	6.5	200	5.3	31	7
Transport, Sv					
Pseudostress, m^2 s^{-2}	2.8	206	2.0	77	29
Longshore	24.5	255	1.5	72	
Offshore	15.6	275	5.9	224	
Mean of four NADW level records (longshore component, cm s^{-1})†	3.4	220	6.4	217	45

*Relative to January 1.
†Moorings 328, instruments 5 and 6, and 340, instruments 4 and 5.

the harmonics is in August, and combined seasonal amplitude is 3.7 Sv. Taking 3-month means at around the time of maximum currents and transports (Figure 5 and 8*a*), June–August, yields 27.8 ± 4.4 Sv, and for the period of minimum transport, December–February, it is 22.0 ± 3.2 Sv (Table 3), yielding an annual range of 5.8 Sv.

Climatological pseudo wind stress (Figure 9*c*) (J. Servain, personal communication, 1991) has a maximum in the alongshore component in summer but about 1 month after the current (Figure 9*a*) and transport (Figure 9*b*) maxima. Further, it has a much more sinusoidal annual cycle than currents and transport, suggesting a role of nonlocal forcing in causing the observed seasonality.

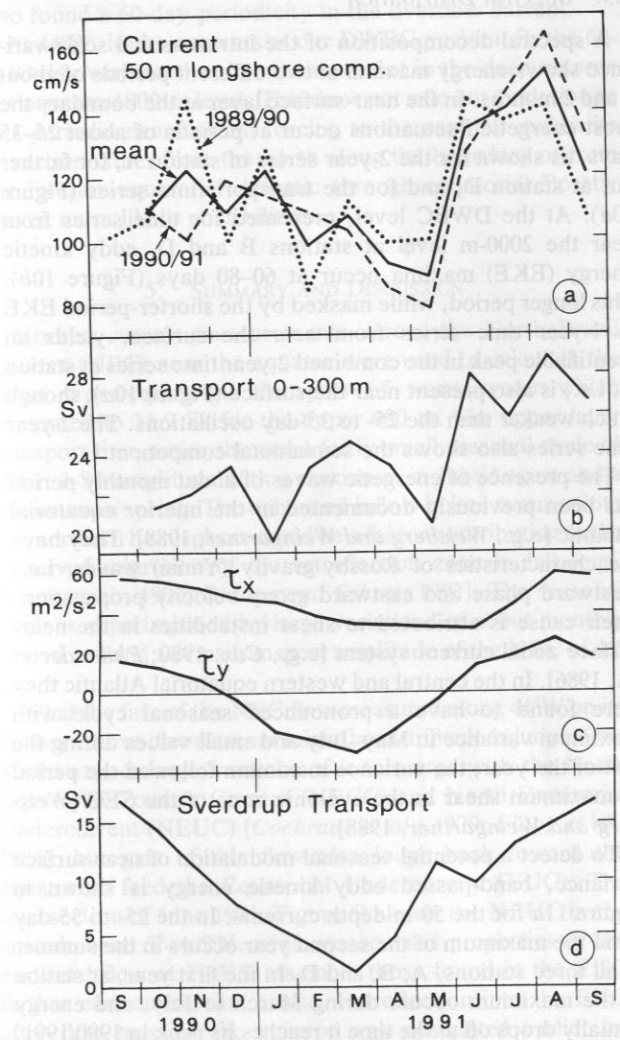

Fig. 9. Monthly means of (*a*) 50-m current (alongshore comparison) from position A for 1989/1990, 1990/1991, and mean of both years. (*b*) Transport 0–300 m. (*c*) Mean climatological pseudo-wind stress; westward (τ_x) and northward (τ_y); (J. Servain, personal communication, 1991). (*d*) Boundary current required by cross-equatorial Sverdrup transport.

4.2. *NADW Layer*

At the upper NADW level a decrease and even reversal of the DWBC occur in April and again in late May to June of the second year (Figure 2*b*). It is interesting to note that this period of general weak upper NADW transport occurs almost simultaneously with that in the deep current core at station D (Figure 2*d*) that was separated, in the distribution of the means and in the shipboard measurements, from the upper NADW core along the continental slope by near-zero means of deep velocity at station C (Figure 3). A similar weak phase of both current cores occurs at the beginning of the time series (Figures 2*b* and *d*). Mooring 328 at position C, deployed during the previous year, did not show any such longer-period current changes. Transport fluctuations of the DWBC associated with these variations can be substantial. Repeating the transport calculation for the NADW (depth range 1000–3250 m) as described above for the means yields 18.0 Sv for an average over 2 months of the high-current period, February 1 to April 1 1991, and 9.7 Sv for the low-current period, April 15–June 15 (Figure 2*b*), using linear decay toward the topography and a decay to the mean profile used previously for station C toward the offshore side. On even shorter periods, on the time scale of a few weeks, fluctuations of transport would be even higher.

The near-equatorial complexity of NADW circulation is more clearly emphasized by the floats of RS93. Some crossed the equator at swift speeds near the boundary and continued southeastward for more than 100 km before looping back toward the equator and then eastward for a while, or continuing southward. After first passing the array in March 1990 near 1°N, one float recirculated northwestward near 3°N and then passed the array a second time in early August. This and our ship sections that showed multiple DWBC cores and eastward recirculation cores explain why freon maxima are found in various "bullets" along the 44°W section (M. Rhein, personal communication, 1992).

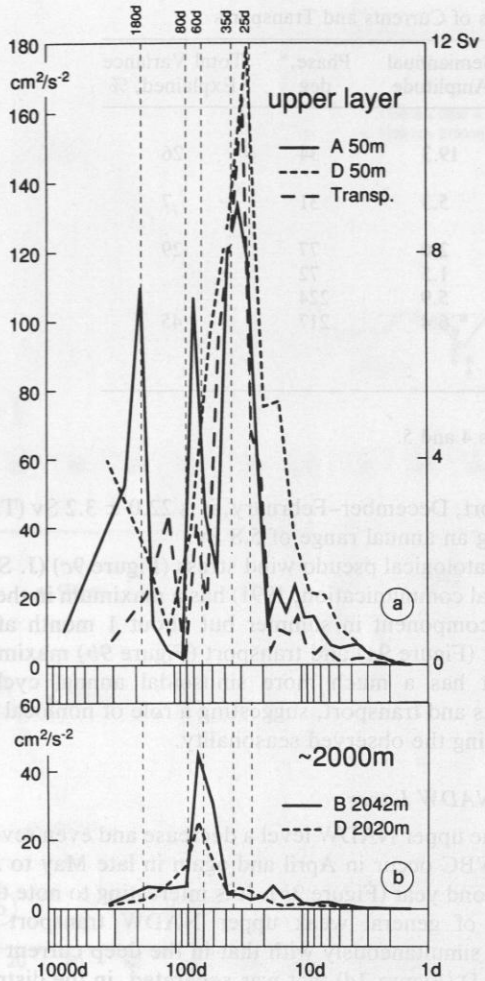

Fig. 10. (*a*) Variance conserving spectrum of eddy kinetic energy from near the surface (50-m depth) for combined 2-year time series of station A and from station D and for transport time series of Figure 5. (*b*) Same as Figure 10*a* but for DWBC at 2000-m level.

Is there an annual cycle in the currents at the DWBC level as seasonally forced high-resolution model results [*Böning and Schott*, 1993] suggest? Annual and semiannual harmonic amplitudes of 5–10 cm s^{-1} result from the sequence of southward maximum in December–March, minimum in March–May, and subsequent weaker maximum again in the 1745- to 2637-m depth records at station B (Figure 2*b*) and the deep currents at station D, but it is reasonable to assume that this sequence is coincidental. In the preceding year, at station C (Figure 2*c*), annual and semiannual harmonics were only 2–4 cm s^{-1}. The question here is, How small an annual cycle could be hidden in the shorter-period eddy noise? An average of two records each out of the DWBC of stations B and C (i.e., from two different years of fairly closely spaced stations (Figure 1*b*) yields an annual harmonic amplitude of 3.4 cm s^{-1} and a semiannual amplitude of 6.4 cm s^{-1} (Table 3). This result is dominated by the higher amplitudes of the station B data, but it is interesting to note that the mean and annual harmonic phase of the four records corresponds (within its error of about 1 month) to that of the near-surface flow (Table 3) and agrees for the two consecutive years. This agreement does not hold for the semiannual component.

Averaging all deep records of stations B, C, and D together reduces the harmonic mean amplitudes further, but one might object that a real seasonal cycle might have a vertical and cross-slope phase and amplitude structure that would also be averaged down by this method. In summary, one cannot rule out a seasonal cycle of a few centimeters per second at depth, but definite proof of its existence requires additional evidence.

Eddy kinetic energy (taken from Table 1) at the upper NADW level is shown in Figure 7*b* in comparison with a cross-stream profile at 1800 m determined by RS93 from SOFAR float displacements. There is a general agreement that mean values fall off from about 200 cm^2 s^{-2} near the current core to <100 cm^2 s^{-2} away from the DWBC. Maximum eddy kinetic energy of the DWBC is observed at the 1745-m level, while mean speeds peak above that depth and below (see also Figure 2*b*). At this depth the flow even reverses periodically, apparently dividing the DWBC vertically into two cores, as also observed in the shipboard profiling sections.

4.3. *Spectral Distribution*

A spectral decomposition of the intraseasonal scale variance shows energy maxima at two different periods of about 1 and 2 months. In the near-surface layer at the boundary the most energetic fluctuations occur at periods of about 25–35 days, as shown for the 2-year series of station A, for farther out at station D, and for the transport time series (Figure 10*a*). At the DWBC level, presented for time series from near the 2000-m level at stations B and D, eddy kinetic energy (EKE) maxima occur at 60–80 days (Figure 10*b*). This longer period, while masked by the shorter-period EKE in 1-year time series from near the surface, yields an identifiable peak in the combined 2-year time series at station A, i.e., is also present near the surface (Figure 10*a*), though much weaker than the 25- to 35-day oscillations. The 2-year time series also shows the semiannual component.

The presence of energetic waves of about monthly period has been previously documented in the interior equatorial Atlantic [e.g., *Weisberg and Weingartner*, 1988]. They have the characteristics of Rossby-gravity (Yanai) waves, i.e., westward phase and eastward group velocity propagation. Their cause is attributed to shear instabilities in the near-surface zonal current system [e.g., *Cox*, 1980; *Philander et al.*, 1986]. In the central and western equatorial Atlantic they were found to have a pronounced seasonal cycle with maximum variance in May–July and small values during the rest of the year; the variance maximum followed the period of maximum shear in the cyclonic zone of the SEC [*Weisberg and Weingartner*, 1988].

To detect a potential seasonal modulation of near-surface variance, band-passed eddy kinetic energy is shown in Figure 11*a* for the 50-m-depth currents. In the 25- to 35-day band the maximum of the second year occurs in the summer at all three stations, A, B, and D. In the first year, at station A the maximum occurs during March to July, and energy actually drops off at the time it reaches its peak in 1990/1991. Measurements for both years agree, though, in that low 25- to 35-day variance is obtained during November–January, but a possible relation to the seasonal variation farther east requires further investigation. Fluctuations observed near 8°N by J90 show energy maxima at 40–60 days with vari-

ances exceeding 200 cm^2 s^{-2} (taking half of their north component variance as roughly equal to total EKE) for the near-surface variations. This period falls in between the 25- to 35-day period variations and the longer-period energy maximum of our observations.

The 60- to 80-day variance (Figure 11*b*) is generally lower near the surface than that at the monthly period, as also shown by the spectra (Figure 10) and does not suggest a consistent annual cycle in the near-surface layer. At A it obtains its maximum during the first several months of the 2-year time series and then is low for the remaining time period, while the offshore station D suggests high values in fall to winter and a minimum in summer.

Johns et al. [1993] also found a dominant 60-day period in the deep variability, different from the 40- to 60-day peak farther up in the water column. The maximum variance at that period in their DWBC records occurred near the bottom and, as one possible cause for that periodicity besides it being imported with the boundary current from the north, was seen a coupling to the inflow of bottom water over the Ceara sill connecting the Ceara Rise with the Mid-Atlantic Ridge near 4°N where *Whitehead and Worthington* [1982] also found a 60-day periodicity in the overflow current.

At 44°W, in the currents at our DWBC position B, the 60- to 80-day variance has its maximum not in the deep records but near the 1800-m level. This does not rule out a relation to this periodic near-bottom forcing to the east but makes its advection either from the north along the boundary or from the interior equatorial Atlantic through equatorial Rossby waves more likely possibilities.

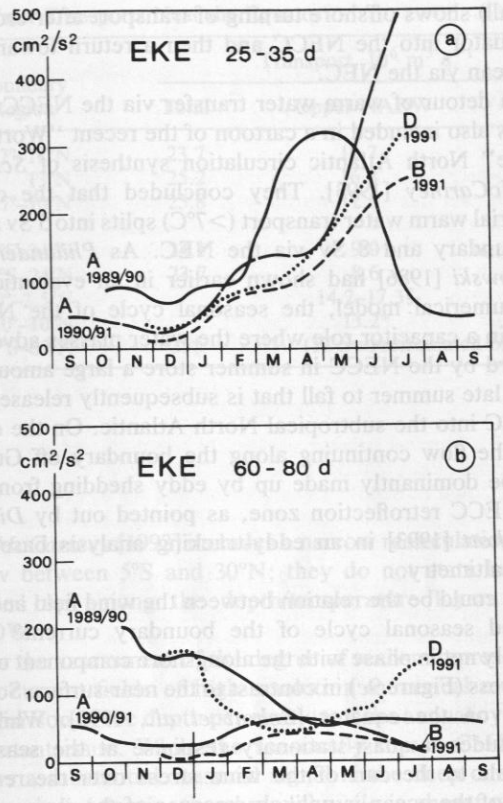

Fig. 11. Band-passed eddy kinetic energy (EKE) for 50-m level currents calculated for running 90-day time intervals (*a*) in 25- to 35-day band and (*b*) 60- to 80-day band.

5. Summary and Discussion

Moored current measurements across the North Brazil Current (NBC) near the equator were used to calculate the mean cross-equatorial transport of warm water which amounted to 31.9 Sv for the upper 600 m. The upper layer transport time series showed a fairly small seasonal cycle of about 3-Sv amplitude with a maximum in July/August and a minimum in spring. The enhanced inflow in late summer into the northern hemisphere could be a factor contributing to the observed migration of the retroflection zone in fall [e.g., *Johns et al.*, 1990; *Didden and Schott*, 1993]. The seasonal cycle is superimposed by large variations of about monthly period causing an rms transport amplitude of the NBC of 4.6 Sv.

What the fate of the NBC flow measured along 44°W on its further course downstream might be is difficult to judge. One would expect large fractions of it to merge with the North Equatorial Counter Current (NECC) and North Equatorial Undercurrent (NEUC) [*Cochrane et al.*, 1979; *Flagg et al.*, 1986], but part of this flow also loops back toward the equator to feed the Equatorial Undercurrent (EUC). The ship section of June 1991 (Figure 6) shows the NEUC in the latitude band 3°–4.5°N, while water mass properties of the eastward flow at 2°–3°N resemble those found in the EUC farther east during that cruise. Retroflection into the EUC after first crossing the equator was postulated earlier by *Metcalf and Stalcup* [1967] based on the oxygen maximum associated with the EUC. A retroflection of the NBC into the EUC also occurs in the high-resolution WOCE-CME simulation [*Schott and Böning*, 1991]. There, however, this retroflection occurs in the longitude zone 38°–44°W, i.e., mostly east of our array location. Following *Schmitz and Richardson* [1991], the net cross-equatorial warm water transfer above 7°C is only 13 Sv, which would suggest that the major part of the boundary flow measured by our array would have to merge with the EUC and eventually recirculate into the southern hemisphere.

It is not clear at the present time how far south the recently discovered coastal undercurrent extends that was postulated first by *Schott and Böning* [1991] based on the CME model analysis and confirmed in the historical data analysis of E. Johns and R. L. Molinari (personal communication, 1992). In the model it extends to the equator in winter when the NECC is absent and supplies part of the EUC flow, while in the climatological geostrophic shears and water mass distributions its southern limit is the NEUC, i.e., about 3°N. Southeastward subsurface flow is not consistently observed in our upper layer records (Figure 2*a*); whether the mean offshore component observed in winter at station D (Figure 3*b*) carries any ingredients of northern origin needs further exploration.

Comparing observed upper layer boundary currents north of the equator to the Sverdrup circulation, one notices an apparent agreement: Sverdrup theory would require a northward boundary current across the equator but a southeastward boundary current north of about 8°N to supply the NECC in latitude range 5°–10°N. This may explain the lack of confirmed significant transport observations directed toward the Caribbean along the boundary, a fact also found in the CME model evaluation of *Schott and Böning* [1991]. Instead, the CME model mean transport function for the upper 1250 m (upwelling through that interface was found to

be small) shows offshore turning of transport after crossing the equator into the NECC and then a return toward the Caribbean via the NEC.

Such detour of warm water transfer via the NECC/NEC route is also included in a cartoon of the recent "Worthington-like" North Atlantic circulation synthesis of *Schmitz and McCartney* [1993]. They concluded that the cross-equatorial warm water transport (>7°C) splits into 5 Sv along the boundary and 8 Sv via the NEC. As *Philander and Pacanowski* [1986] had shown earlier in an evaluation of their numerical model, the seasonal cycle of the NECC serves in a capacitor role where the water masses advected eastward by the NECC in summer store a large amount of heat in late summer to fall that is subsequently released via the NEC into the subtropical North Atlantic. On the other hand, the flow continuing along the boundary off Guiana could be dominantly made up by eddy shedding from the NBC/NECC retroflection zone, as pointed out by *Didden and Schott* [1993] in an eddy-tracking analysis based on Geosat altimetry.

What could be the relation between the wind field and the observed seasonal cycle of the boundary current? It is obviously not in phase with the alongshore component of the wind stress (Figure 9*c*) in contrast to the near-surface Somali Current on the equator [*Schott et al.*, 1990]. While at mid-latitudes a quasi-stationary response at the seasonal time scale to the curl of the wind stress over the remote interior of the ocean is unlikely because of the slow propagation speed of the Rossby waves that carry the baroclinic seasonal signal; this reason should not apply near the equator. However, the observed small seasonal cycle of the NBC on the equator is in apparent disagreement with straightforward application of the Sverdrup transport hypothesis, which would require, based on *Hellermann and Rosenstein* [1983] wind stress, a fairly large boundary current seasonal cycle, ranging from 17 Sv northward in September to just 1.5 Sv in March (Figure 9*d*). The reason for the large variation of the wind stress curl field and derived Sverdrup transport is the seasonal meridional transition of the Intertropical Convergence Zone, which is located between 3°N and 8°N in summer and near the equator in winter. Consequently, the clockwise equatorial gyre straddles the equator in late summer with maximum western boundary transport across the equator and is shifted to the south in winter with correspondingly small western boundary transports on the equator (Figure 9*d*). Of course, one cannot expect a purely wind-driven response in the western boundary transports due to the superposition with the vertical thermohaline cell and possible nonlinear coupling. Yet the smallness of the seasonal cycle in the boundary current transport in comparison with Sverdrup dynamics is somewhat surprising and needs further study where evaluation of numerical model fields can play a useful role.

Whether the seasonal cycle is driven by seasonal zonal inflow to variation from the SEC is not clear. Ship drifts of the SEC just north of the equator show a westward maximum in July/August, while for the SEC branch south of the equator the ship drift currents do not suggest a clear seasonal cycle [*Arnault*, 1987]. A recent evaluation of geostrophic surface currents from Geosat altimetry [*Romaneessen*, 1993] showed a westward maximum of the SEC branch in the 2°–5°S latitude range in June, which would lead the boundary current cycle at 44°W derived here by 1–2 months.

The cross-equatorial exchange of Antarctic Intermediate Water (AIW) that should spread northward along the boundary in the 600- to 900-m depth range could not be determined because of sparse coverage of the array, but mean northwestward flow along the boundary of 5 cm s^{-1} was recorded in that depth range. Farther out the current reversed to southeastward. This cross-slope profile is in agreement with the current pattern deduced from the 800-m float tracks by *Richardson and Schmitz* [1993], who concluded an offshore counterflow to the northwestward AIW boundary current that they find feeding into a broad eastward flow (during the observational period) in the equatorial belt.

The mean flow at the upper and middle NADW depth range in our current meter section is found to be confined to the topography. Using the cross-slope profile determined for the 1800-m depth level from float trajectories, a mean transport of 14.2 Sv is determined for the depth range 1000–3100 m. Using an extrapolation suggested by our ship measurements along 44° gives a wider core of the DWBC, resulting in a transport of 17.0 Sv, similar to the 17.6 Sv obtained when using an exponential cross-shore current profile with 30-km decay scale; for a position farther north *Johns et al.* [1993] obtained good comparison of single mooring transports for the DWBC below 2500 m with geostrophic calculations by *Molinari et al.* [1992].

Whether and where part of the upper DWBC branches off along the equator cannot be determined from our measurements. Floats deployed in the DWBC (1800 m) that turned off toward the equator in the RS93 study did so after first crossing the equator southward and proceeding along the boundary to 1°–2°S and then retroflecting back toward the equator. This would suggest that our estimate still includes any part that later may get lost along the equator. On the other hand, whether much mean transport branches off at all is unclear. The CME model evaluation of *Böning and Schott* [1993] showed that the observed equatorial tracer wedge can be accomplished with very weak advection involving only minor branching of the DWBC transport. The RS93 floats in the equatorial zone were slushing back and forth at periods too long to average out in their observations, allowing not much room for conclusions as to the mean advection. The complexity of the near-equatorial boundary current system is also apparent when comparing shipboard profiling sections along 44°W with Pegasus measurements carried out farther north across the DWBC. At 44°W there exist multiple cores at vertical scales of only a few hundred meters, while off French Guiana the vertical scale in individual ship sections is much larger [*Colin et al.*, 1992]. Whether these cores are depth-variable in time and smooth out in yearlong averaging by a current meter array or whether we have an aliasing problem in our moored data interpolation from Figure 4 needs some additional consideration.

Splitting the upper DWBC transport in the depth range 1000–3100 m up into temperature layers (Figure 4) (as *Molinari et al.* [1992] did for their geostrophic transports) yields a reasonable agreement of moored transport (5.4–6.5 Sv) versus geostrophic (5.8 Sv) for the transport in the potential temperature range 2.4°–3.2°C, corresponding to about 2100–3100 m. However, for the transport in the 1000- to 2100-m range, our boundary current estimate of 9.0–10.8 Sv is about double their geostrophic estimate of 4.9 Sv in that temperature class, which results in our total of 14.2–17.3 Sv above 2.4°C compared to their value of 10.7 Sv (Table 4).

TABLE 4. Estimates of North Atlantic Deep Water Transports Near the Equator

References	Method	Boundary Region	Transport, 10^6 m^3 s^{-1} Total	Upper NADW	Lower
Molinari et al. [1992]	Geostrophic (relative θ = 4.7°C)	2°–12°N	23.7	10.7	13.0
		13°N	25.2	16.8	8.4
Speer and McCartney [1991]	Geostrophic (relative θ = 4.7°C)	7°–10°N	25.8	12.6	13.2
Roemmich [1983]	8°S Geostrophic/inverse	24°S–24°N	24.1	9.0	15.1
	8°N Geostrophic/inverse	24°S–24°N	23.7	8.6	15.3
This study	Moored center of mass	0°–2.5°N		14.2–17.3§	(4.5)†
Richardson and Schmitz [1993]	Floats/moored	0°–10°N		13.2*	
Schmitz and McCartney [1993]	"Worthington-type"	5°S–65°N	35‡	(17 Sv recirculated offshore)	

*Above 2800 m.
†South of 2.5°N.
‡In θ = 1.8–4°C range.
§For different extrapolations used (see text).

A comparison with evaluations of earlier section data from 7°–10°N [*Speer and McCartney*, 1991] and inversion results of *Roemmich* [1983] generally support the lower value of *Molinari et al.* [1992]. As offshore shipboard profiling along 44°W and Freon analysis (M. Rhein, personal communication, 1992) as well as the float measurements of RS93 described above indicate that significant recirculation and DWBC water mass redistribution occur away from the boundary. The high upper DWBC transport value compared to the other measurements farther away from the equator if not due to vertical or horizontal aliasing or interpolation problems suggests a near-equatorial recirculation cell of the order of 5 Sv. This is also supported by the consistent westward current at upper NADW levels between coastal distances of 100 and 180 km (Figure 7*a*).

For the lower NADW range of 1.8°–2.4°C, corresponding to depths of about 3100–4100 m (Figure 4), *Molinari et al.* [1992] obtained 13.1 Sv. Our only evidence from the moored array measurements for transport in that water mass class stems from two deep instruments at station D (Figures 3 and 4). Estimates of the associated transport using interpolation between instruments of the array or the exponential profile with 30-km decay scale result in a value of about 4.5 Sv. The θ = 1.8°C interface between lower NADW and Antarctic Bottom Water is located near 4100 m along 44°W (Figure 4) and the sill depth northwest of the Ceara Rise between 4000 and 4100 m (Figure 1*b*). This should result in much of the lower NADW passing south of Ceara, where a second eastward current core in the depth range of 3100–4100 m appeared to exist in individual shipboard profiling sections at 3°–3.5°N, i.e., beyond the range covered by our moored array. On the other hand, the 1.8°C interface drops significantly to the north, from 4100 m at the equator to 4400 m at 9°N, and it has to be considered that a sizeable amount of lower NADW may also pass to the north of the Ceara Rise. From a recent shipboard profiling section during *Meteor* cruise M22, an estimate of 7 Sv for that transport contribution was obtained. Taking this as representative for the mean would yield a total of 12 Sv of lower NADW transport plus a contribution from a potentially existing mean core near 3°N, i.e., would also arrive at a fairly large total lower NADW transport. What is interesting is that the authors basing their results on near-equatorial hydrographic sections all agree on a high total DWBC transport of about 25 Sv or even higher. The large number of 35 Sv (Table 4) of *Schmitz and McCartney* [1993] includes a narrow recirculation cell of 17 Sv between 5°S and 30°N; they do not state how it is divided up among the depth/temperature layers of the NADW.

For the assessment of the degree of realism represented in deep current fields of high-resolution numerical models, a comparison of the depth penetration of the annual cycle is an important issue. While the seasonally forced CME model shows a substantial seasonal signal in the deep currents of the tropical Atlantic, the seasonal cycle is absent when the model is forced with constant winds over the equator [*Böning and Schott*, 1993]. The amplitude of the model seasonal cycle of 5–10 cm s^{-1} comes mainly from the fact that shorter-period fluctuations in the model are not random from 1 year to the next but occur phase-locked with the annual harmonic, thus adding higher harmonics while the annual and semiannual harmonics themselves are only a few centimeters per second each. This is not larger than the harmonic amplitudes we obtain from averaging different deep records together (Table 3). Hence from our observations we cannot exclude that a deep seasonal cycle as suggested by high-resolution models may exist, but further evidence is required to prove its existence and therewith the realism of deep model variability.

With regard to the periodicity of the intraseasonal fluctuations, the existence of two different periods is interesting. The 1-month period that has its amplitude maximum in the near-surface layer is a well-known periodicity of the interior equatorial Atlantic generated by horizontal shear instability between the NECC and the northern SEC [e.g., *Weisberg and Weingartner*, 1988]. The longer period found here with dominant amplitudes at the upper NADW level was also recently documented at the NADW level farther north by *Johns et al.* [1993]. Its cause is not yet understood. It might be imported in the DWBC along the topography from the north or might even be related in some complicated way to the strong fluctuations of a period of about 2 months observed earlier in the inflow of bottom water east of the Ceara Rise [*Whitehead and Worthington*, 1982]. A likely possibility is that this oscillation is imported from along the equator by equatorial Rossby waves in agreement with the findings from numerical models [e.g., *Böning and Schott*, 1993; *McCreary and Yu*, 1992] that besides the 1-month instability period observed basically in all oceans, longer intraseasonal periods may exist along the equator as well. New measurements

with moored stations are underway on the equator at 35°W and at 44°W near the boundary, which should shed some light on the equatorial connection of this boundary current variability.

Acknowledgments. We thank captains and crews of Research vessels *Meteor and Malcolm Baldrige* for their help with deployments and retrievals of the moored stations and D. Carlsen, C. Meinke, and U. Papenburg for technical assistance. Helpful comments were obtained from M. Rhein, M. Visbeck, and one anonymous reviewer. We appreciate the assistance of A. Eisele, who drafted the figures. Financial support of Deutsche Forschungsgemeinschaft, SFB 133, is gratefully acknowledged.

REFERENCES

Arnault, S., Tropical Atlantic geostrophic currents and ship drifts, *J. Geophys. Res.*, *92*(C5), 5076–5088, 1987.

Böning, C., and F. Schott, Deep currents and the eastward salinity tongue in the equatorial Atlantic: Results from an eddy-resolving, primitive equation model, *J. Geophys. Res.*, *98*(C4), 6991–6999, 1993.

Böning, C. W., R. Döscher, and R. G. Budich, Seasonal transport variation in the western subtropical North Atlantic: Experiments with an eddy-resolving model, *J. Phys. Oceanogr.*, *21*, 1271–1289, 1991.

Candela, J., R. C. Beardsley, and R. Limeburger, Separation of tidal and subtidal currents in ship-mounted acoustic Doppler current profiler observations, *J. Geophys. Res.*, *97*(C1), 769–788, 1992.

Cochrane, J. D., F. J. Kelly, Jr., and C. R. Olling, Subthermocline countercurrents in the western equatorial Atlantic Ocean, *J. Phys. Oceanogr.*, *9*, 724–738, 1979.

Colin, C., J. M. Bore, R. Chuchla, and D. Corre, Programme NOE, resultats de courantométrie (mouillage de subsurface) au point 6°12′N–51°01′W du 31 mars au 18 novembre 1990, *Doc. Sci. 4*, Cent. ORSTOM de Cayenne, Cayenne, French Guiana, 1991.

Colin, C., B. Bourles, J. M. Bore, and P. Y. Noyer, Programme NOE, resultats des observations de courants au Pegasus Campagne NOE/STACS de juin 1991, *Doc. Sci. 6*, Cent. ORSTOM de Cayenne, Cayenne, French Guiana, 1992.

Cox, M. D., Generation and propagation of 30-day waves in a numerical model of the Pacific, *J. Phys. Oceanogr.*, *10*, 1168–1186, 1980.

Didden, N., and F. Schott, Seasonal variations in the western tropical Atlantic: Surface circulation from Geosat altimetry and WOCE model results, *J. Geophys. Res.*, *97*(C3), 3529–3541, 1992.

Didden, N., and F. Schott, Eddies in the North Brazil Current retroflection observed by Geosat altimetry, *J. Geophys. Res.*, in press, 1993.

Fischer, J., and M. Visbeck, Deep velocity profiling with self-contained ADCPs, *J. Atmos. Oceanic Technol.*, in press, 1993.

Flagg, C. N., R. L. Gordon, and S. McDowell, Hydrographic and current observations on the continental slope and shelf of the western equatorial Atlantic, *J. Phys. Oceanogr.*, *16*, 1412–1429, 1986.

Hellerman, S., and M. Rosenstein, Normal monthly wind stress over the world ocean with error estimates, *J. Phys. Oceanogr.*, *13*, 1093–1105, 1983.

Johns, W. E., T. N. Lee, F. Schott, R. Zantopp, and R. Evans, The North Brazil Current retroflection: Seasonal structure and eddy variability, *J. Geophys. Res.*, *95*(C12), 22,103–22,120, 1990.

Johns, W. E., D. M. Fratantoni, and R. J. Zantopp, Deep western boundary current variability off northeastern Brazil, *Deep Sea Res.*, *40*(2), 293–310, 1993.

McCreary, J. P., and Z. Yu, Equatorial dynamics in a 2 1/2 layer model, *Prog. Oceanogr.*, *29*, 61–132, 1992.

Metcalf, W. G., and M. C. Stalcup, Origin of the Atlantic Equatorial Undercurrent, *J. Geophys. Res.*, *72*(20), 4959–4974, 1967.

Molinari, R. L., R. A. Fine, and E. Johns, The deep western boundary current in the tropical North Atlantic Ocean, *Deep Sea Res.*, *39*(11/12), 1967–1984, 1992.

Philander, G., and R. C. Pacanowski, The mass and heat budget in a model of the tropical Atlantic Ocean, *J. Geophys. Res.*, *91*(C12), 14,212–14,220, 1986.

Philander, S. G. H., W. J. Hurlin, and R. C. Pacanowski, Properties of long equatorial waves in models of the seasonal cycle in the tropical Atlantic and Pacific oceans, *J. Geophys. Res.*, *91*(C12), 14,207–14,211, 1986.

Ponte, R. M., J. Luyten, and P. L. Richardson, Equatorial deep jets in the Atlantic Ocean, *Deep Sea Res.*, *37*(4), 711–713, 1990.

RD Instruments, Acoustic Doppler current profilers, principles of operation: A practical primer, San Diego, Calif., 1989.

Reid, J. L., On the total geostrophic circulation of the South Atlantic Ocean: Flow patterns, tracers, and transports, *Prog. Oceanogr.*, *23*, 149–244, 1989.

Richardson, P. L., and S. G. H. Philander, The seasonal variations of surface currents in the tropical Atlantic Ocean: A comparison of ship drift data with results from a general circulation model, *J. Geophys. Res.*, *92*, 715–724, 1987.

Richardson, P. L., and G. Reverdin, Seasonal cycle of velocity in the Atlantic North Equatorial countercurrent measured by surface drifters, current meters, and ship drifts, *J. Geophys. Res.*, *92*, 3691–3708, 1987.

Richardson, P. L., and W. J. Schmitz, Deep cross-equatorial flow in the Atlantic measured with SOFAR floats, *J. Geophys. Res.*, 98(C5), 8371–8387, 1993.

Richardson, P. L., and D. Walsh, Mapping climatological seasonal variations of surface currents in the tropical Atlantic using ship drift data, *J. Geophys. Res.*, *91*, 10,537–10,550, 1986.

Roemmich, D., The balance of geostrophic and Ekman transports in the tropical Atlantic Ocean, *J. Phys. Oceanogr.*, *13*, 1534–1539, 1983.

Roemmich, D. H., and C. Wunsch, Two transatlantic sections: Meridional circulation and heat flux in the subtropical North Atlantic Ocean, *Deep Sea Res.*, *32*(6), 619–664, 1985.

Romaneessen, E., Untersuchungen saisonaler Varibailität im südlichen äquatorialen Atlantik und der Karibik mit Geosat, diplomarbeit, Univ. Kiel, Kiel, Germany, 1993.

Schmitz, W. J., Jr., and M. S. McCartney, On the North Atlantic circulation, *Rev. Geophys.*, *31*, 29–49, 1993.

Schmitz, W. J., Jr., and P. L. Richardson, On the sources of the Florida Current, *Deep Sea Res.*, *38*, suppl. 1, 379–409, 1991.

Schott, F., and C. W. Böning, The WOCE model in the western equatorial Atlantic: Upper layer circulation, *J. Geophys. Res.*, *96*(C4), 6993–7004, 1991.

Schott, F., J. C. Swallow, and M. Fieux, The Somali Current at the equator: Annual cycle of currents and transports in the upper 1000 m and connection to neighbouring latitudes, *Deep Sea Res.*, *37*, 1825–1848, 1990.

Speer, K. G., and M. S. McCartney, Tracing lower North Atlantic deep water across the equator, *J. Geophys. Res.*, *96*(C11), 20,443–20,448, 1991.

Stramma, L., Geostrophic transport of the South Equatorial Current in the Atlantic, *J. Mar. Res.*, *49*, 281–294, 1991.

Tsuchiya, M., Thermostads and circulation in the upper layer of the Atlantic Ocean, *Prog. Oceanogr.*, *16*, 235–267, 1986.

Weisberg, R. H., and T. J. Weingartner, Instability waves in the equatorial Atlantic, *J. Phys. Oceanogr.*, *18*, 1641–1657, 1988.

Weiss, R. F., J. L. Bullister, R. A. Van Woy, J. M. Warner, P. K. Salameh, and R. H. Gammon, Transient tracers in the ocean, in Tropical Atlantic Study: Fluorochlorocarbon Measurements, *Rep. 91-1*, 159 pp., Scripps Inst. of Oceanogr., La Jolla, Calif., 1991.

Whitehead, J. A., Jr., and L. V. Worthington, The flux and mixing rates of antarctic bottom water within the North Atlantic, *J. Geophys. Res.*, *87*(C10), 7903–7924, 1982.

J. Fischer, J. Reppin, F. Schott, and V. Send, Institut für Meereskunde, Universität Kiel, Düsternbrooker Weg 20, D-24105 Kiel 1, Germany.

(Received November 10, 1992;
revised April 19, 1993;
accepted April 28, 1993.)